

Structural and Vibrational Properties of Imidazo[4,5-*c*]pyridine, a Structural Unit in Natural Products

Lucyna Dymińska,^{*,†} Zbigniew Węgliński,[†] Anna Gağor,[‡] and Jerzy Hanuza^{†,§}

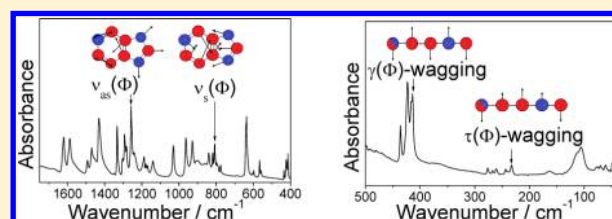
[†]Department of Bioorganic Chemistry, Institute of Chemistry and Food Technology, Faculty of Engineering and Economics, Wrocław University of Economics, Komandorska 118/120, 53-345 Wrocław, Poland

[‡]Department of Crystallography, Institute of Low Temperature and Structure Research, Polish Academy of Sciences, 50-422 Wrocław, Poland

[§]Department of Solid State Spectroscopy, Institute of Low Temperature and Structure Research, Polish Academy of Sciences, 50-422 Wrocław, Poland

S Supporting Information

ABSTRACT: The molecular structures and vibrational properties of 1*H*-imidazo[4,5-*c*]pyridine in its monomeric and dimeric forms are analyzed and related to the experimental results derived from the XRD, IR, and Raman studies. The theoretical data are discussed on the basis of DFT quantum chemical calculations using the B3LYP correlation functional and 6-311G(2d,2p) basis set. This compound crystallizes in the non-centrosymmetric orthorhombic space group *Fdd2*. The asymmetric unit contains one molecule of 1*H*-imidazo[4,5-*c*]pyridine and disordered molecules of solvents. The molecules are organized in hydrogen-bonded chains propagating along the [1 0 $\bar{3}$] direction. The stability of the dimeric form arising from charge delocalization and the existence of an N–H...N intermolecular hydrogen bond has been analyzed using the natural bond orbital approach. The normal modes, which are unique for the imidazopyridine skeleton, have been identified. The spectra of other compounds containing the imidazopyridine unit have been analyzed.



The imidazopyridines (IP) are a class of hypnotic and antibacterial drugs related to benzodiazepines.^{1,2} Ageladine A and its analogues constitute a class of IPc (imidazo[4,5-*c*]pyridine) derivatives. Ageladine A has been reported to inhibit various subtypes of matrix metalloproteinases. The compound is believed to accompany inflammatory diseases caused by macrophage infiltration such as skin diseases,^{3–5} atherosclerosis,⁶ aneurysms,⁷ and cancers.^{8–10}

Imidazo[4,5-*c*]pyridine (or 3-deazapurine) is a framework that has found significant applicability in antiviral agent design and biochemical investigations.^{11,12} Deazapurine derivatives have been shown to possess biological activity as adenosine receptor ligands,¹³ antitumor agents,¹⁴ and enzyme inhibitors.¹⁵ Carbocyclic analogues of 3-deazapurines such as 3-deazaaristeromycin and 3-deazaneplanocin A hydrochloride (DZNep) are potential inhibitors of *S*-adenosylhomocysteine hydrolase, which displays a wide variety of antiviral activity against DNA and RNA viruses.^{16–18} 3-Deazapurine may form a ligand-binding core of corticotrophin releasing factor (CRF) receptor. CRF is implicated in major neuropsychiatric disorders, such as anxiety-related disorders (panic disorders), post-traumatic stress disorders, and depression.^{19–22} 3-Deazaadenosine (DZA), possessing antiviral activity and anti-inflammatory properties,²³ or ABT-491 hydrochloride (ABT-491), a platelet-activating factor receptor antagonist (PAF), which may be an important mediator of allergic rhinitis,²⁴ are other compounds containing the imidazopyridine skeleton.

In our previous papers molecular structures, vibrational energy levels, and potential energy distributions of methyl derivatives of imidazo[4,5-*c*]pyridine,²⁵ imidazo[4,5-*b*]pyridine,²⁶ and its methyl derivatives were studied.²⁷ This paper reports studies on the molecular structures and vibrational properties of imidazo[4,5-*c*]pyridine that occur in several natural products and the aforementioned pharmaceuticals as a basic skeleton. The assignment of the observed IR and Raman bands to the respective normal modes is proposed on the basis of DFT quantum chemical calculations. We also show that the two-ring IP systems give rise to characteristic vibrations.

RESULTS AND DISCUSSION

Crystal Data of {Imidazo[4,5-*c*]pyridine}₄·C₂H₅OH·6H₂O. C_{6.5}H_{9.5}N₃O_{1.75}, *M_r* = 157.67, orthorhombic crystal system, space group *Fdd2*, *Z* = 16, *a* = 22.652(2) Å, *b* = 34.834(2) Å, *c* = 3.7178(2) Å, *U* = 2933.6(3) Å³, 6170 reflections measured, 1378 unique (*R_{int}* = 0.032). The final *R*(*F*² > 2σ(*F*²)), *wR*(*F*²) values are 0.044 and 0.127, respectively. Goodness of fit *S* = 1.034, electron density from difference Fourier map: ρ_{max} = 0.322, ρ_{min} = −0.232 e/Å³. The final coordinates (×10⁵) and *U*_{iso} (×10⁴) of the IPc atoms are as follows: N1 27957(8), 4587(5), 1936(6), 337(5); C2

Received: April 16, 2013

Published: September 6, 2013

22657(10), 4853(6), 3332(7), 323(6); N3 20439(8), 8483(5), 3449(5), 281(5); C4 25156(9), 14746(7), 1475(6), 297(5); C5 30392(10), 15997(7), 1(6) 323(8); N6 34980(8), 13693(6), 923(5), 323(5); C7 34422(9), 9934(7), 412(6), 315(6); C8 29376(9), 8372(6), 1076(6), 278(5); C9 24693(8), 10812(6), 2029(6), 249(5).²⁸

Crystal Structure of {Imidazo[4,5-*c*]pyridine}₄·C₂H₅OH·6H₂O (IPc). IPc crystallizes in the orthorhombic non-centrosymmetric *Fdd2* space group. An asymmetric unit contains one molecule of imidazo[4,5-*c*]pyridine and disordered molecules of solvents. There are 0.25 molecule of EtOH and 1.5 molecules of H₂O per IPc molecule in the crystal structure. All atoms of the IPc molecule adopt general 16*b* Wyckoff positions of C₁ symmetry. The molecular structure along with the atom-labeling scheme is presented in Figure 1.

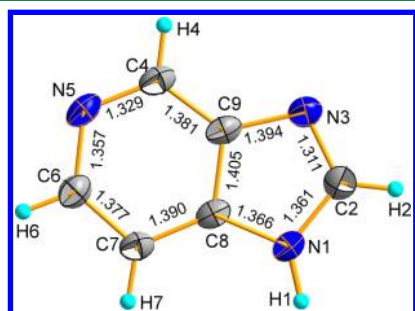


Figure 1. Molecule of imidazo[4,5-*c*]pyridine in the crystal structure of IPc, *T* = 110 K.

The conformation of IPc is similar to that of IPb,²⁶ 4MIPc, and 7MIPc crystals.²⁵ The molecule is nearly planar; the planes of the imidazole and pyridine rings intersect at a 1.37° angle. The valence angles between non-hydrogen atoms of pyridine are in the range 115.8(2)–125.0(2)°; the limiting angles are for C(6)–C(7)–C(8) and N(5)–C(6)–C(7), respectively. As in 4MIPc and 7MIPc the C(4)–N(5) bond may be considered as a double bond. In the imidazole ring a double bond of 1.311(3) Å is found between N(3) and C(2) atoms.

Molecules of IPc are organized in hydrogen-bonded chains propagating along the [1 0 $\bar{3}$] direction. Strong N(1)–H(1)⋯N(5) hydrogen bond interactions with a donor to acceptor distance of 2.816(3) Å and donor-to-acceptor angle of 174(3)° form a 1-D hydrogen bond network. The dihedral angle between two hydrogen-bonded molecules is equal to 12.9°. Simultaneously, π – π interactions organize the hydrogen-bonded chains in stacks along the *c* direction. Molecules involved in these interactions are arranged parallel to each other, although the centers of adjacent molecules are shifted 1.19(1) Å in the plane of the ring. The ring separation distance is equal to 3.39(1) Å. Additionally, the N-3 atoms from the imidazole ring participate in C–H⋯N contacts with the C-2 imidazole carbon from neighboring chains. These weak interactions with a C–N distance of 3.55(1) Å and a C–H–N angle of 143(1)° together with π – π and N–H⋯N bonds play a major role in the spatial organization of molecules.

There are large voids in the crystal structure between the chains that are filled with disordered molecules of EtOH and H₂O, solvents that were used in the crystallization process. It is possible that some H₂O molecules act as hydrogen bond donors with a nitrogen from IPc since there is one bonding distance between N-3 and O(3_w) atoms equal to 2.88(1) Å. Figure 2(a) presents the crystal packing of IPc in the unit cell.

Figure 2(b) shows N–H⋯N, C–H⋯N, and π – π interactions, which build a three-dimensional crystal structure.

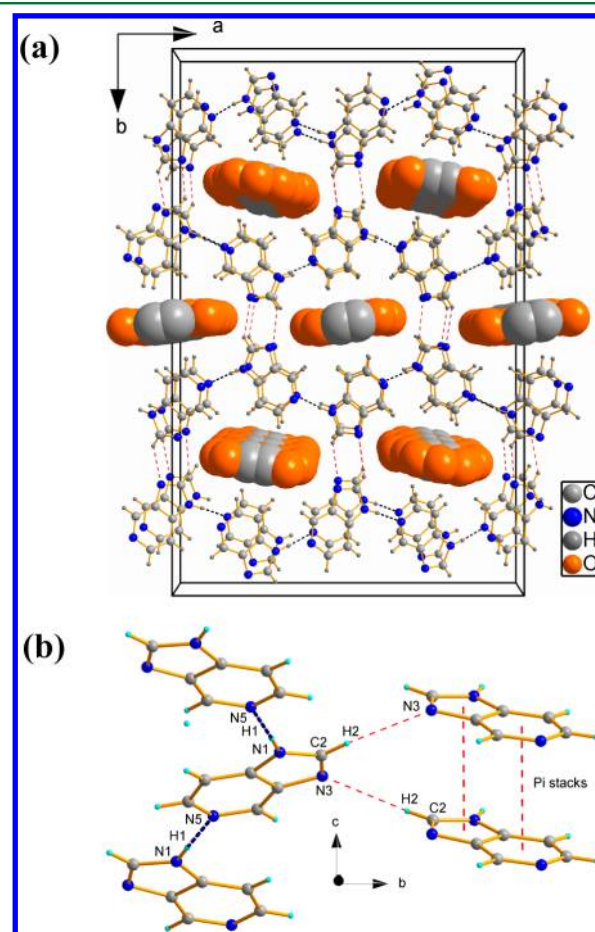


Figure 2. (a) Crystal packing of {imidazo[4,5-*c*]pyridine}₄·C₂H₅OH·6H₂O as seen from the *c* direction. Large voids in the crystal structure are filled with disordered molecules of solvents (water and ethanol), here presented in a space-filling model. Dashed, navy lines stand for hydrogen N–H⋯N bonds, and dashed red lines represent C–H⋯N contacts. (b) Intermolecular N–H⋯N, C–H⋯N, and π – π interactions determining the crystal packing.

Molecular Structure of 1*H*-Imidazo[4,5-*c*]pyridine. The IPc skeleton appears as a main fragment in several important biochemical compounds such as 3-deazaaristeromycin, 3-deazaplanocin A, and 3-deazaadenosine.^{6–8,29} Theoretical calculations have been performed for the optimized geometry of IPc. The structural parameters obtained from the optimization of IPc in its monomeric and dimeric forms are listed in Table 1 together with its X-ray data. The atom-numbering scheme for the molecule is given in Figure 1.

Table 1 shows that the bond lengths and angles calculated for IPc are in good agreement with the experimental values obtained from XRD studies. The largest difference between experimental and calculated bond lengths and angles is 0.019 Å and 1.16°, respectively.

These data can be compared to the experimental values of bond lengths and bond angles taken from our previous papers.^{25–27}

Normal Modes of the 1*H*-Imidazo[4,5-*c*]pyridine. The calculated and experimental wavenumbers of IPc are listed in Table 2. The theoretical and experimental spectra are presented

Table 1. Comparison of the Calculated Geometrical Parameters for 1*H*-Imidazo[4,5-*c*]pyridine Monomer and Dimer with Experimental X-ray Data^a

	optimized parameters from DFT data B3LYP 6-311G(2d,2p)			crystal structure of IPc
	IPc monomer	IPc dimer		
		molecule I	molecule II	
Bond Lengths (Å)				
N(1)–C(2)	1.379	1.374	1.380	1.361(3)
C(2)–N(3)	1.301	1.306	1.301	1.311(3)
N(3)–C(9)	1.389	1.387	1.386	1.394(3)
C(9)–C(8)	1.408	1.41	1.410	1.405(3)
C(8)–N(1)	1.376	1.373	1.374	1.366(3)
C(9)–C(4)	1.395	1.395	1.392	1.381(3)
C(4)–N(5)	1.328	1.329	1.331	1.329(3)
N(5)–C(6)	1.347	1.348	1.349	1.357(3)
C(6)–C(7)	1.387	1.386	1.384	1.377(3)
C(7)–C(8)	1.391	1.392	1.390	1.390(3)
Bond Angles (deg)				
N(1)–C(2)– N(3)	113.61	113.61	114.31	114.6(2)
C(2)–N(3)– C(9)	104.56	104.51	104.10	103.6(2)
N(3)–C(9)– C(8)	110.53	110.59	110.31	109.9(2)
C(9)–C(8)– N(1)	104.64	104.60	105.19	105.7(2)
C(8)–N(1)– C(2)	106.66	106.69	106.09	106.2(2)
C(8)–C(9)– C(4)	118.42	118.54	118.51	119.2(2)
C(9)–C(4)– N(5)	121.54	121.00	121.67	121.6(2)
C(4)–N(5)– C(6)	118.75	119.46	118.60	118.3(2)
N(5)–C(6)– C(7)	125.13	124.59	125.16	125.0(2)
C(6)–C(7)– C(8)	115.35	115.48	115.57	115.8(2)
C(7)–C(8)– C(9)	120.81	120.93	120.51	120.2(2)
N–H...N		2.950		2.816(3)
∠(N–H...N)		178.50		174(3)

^aThe molecular structure and atom-numbering scheme are shown in Figure 1.

in Figures 3 and 4. The assignments of the modes have been performed on the basis of DFT calculations and the potential energy distribution (PED) as well as by analogy to the spectra of IPc derivatives.²⁵ The correlation graphs of the experimental and calculated wavenumbers are presented in Figure 5, showing their good agreement.

1*H*-Imidazo[4,5-*c*]pyridine of the formula C₆H₅N₃ reveals 36 vibrational degrees of freedom. Fifteen normal modes correspond to stretching modes [$\nu(\text{NH})$, 4 $\nu(\text{CH})$, and 10 $\nu(\phi)$], and 21 bending modes are subdivided into 10 in-plane and 11 out-of-plane modes. Table 2 lists the calculated wavenumbers for the IPc skeleton together with the PED data and assignment. These results are used in the discussion of the vibrational modes of the IPc and their assignment to the characteristic vibrations of this unit. The modes can be subdivided into vibrations in which only the pyridine ring (ϕ_p) is involved, vibrations in which only the imidazole ring

(ϕ_I) participates, and the modes of mixed nature, in which both rings vibrate in a concerted motion.

In-Plane Modes of IPc. Twenty-five in-plane vibrations of the IPc can be identified as ν_1 – ν_{19} , ν_{21} , ν_{23} , ν_{26} , ν_{29} , ν_{31} , and ν_{33} . The $\nu(\text{CH})$ stretching vibrations of a heteroaromatic structure are expected to appear in the 3000–3100 cm^{−1} wavenumber range. We assigned these vibrations to the four bands observed at 3014–3125 cm^{−1} (see Figures 3 and 4). It should be noted that the $\nu(\text{CH})_I$ vibrations of the imidazole ring appeared at higher wavenumbers than the $\nu(\text{CH})_p$ vibrations of the pyridine ring.

The $\nu(\Phi)$ stretching vibrations are observed in the 1000–1624 cm^{−1} range (Φ denotes the whole imidazopyridine skeleton, i.e., $\phi_p + \phi_I$ system). Some vibrations lying below 1500 cm^{−1} also have a significant contribution of the $\delta(\text{CH})$ in-plane bending vibrations.

The six in-plane bending vibrations of the Φ skeleton are located in the 400–929 cm^{−1} range. These modes can be divided into nearly pure vibrations of the pyridine or imidazole ring or mixed vibrations of the both rings. The band at 928–929 cm^{−1} belongs to the nearly pure imidazole ring vibration $\delta(\phi_I)$. The mode at about 560 cm^{−1} is an example of the nearly exclusive pyridine ring vibration $\delta(\phi_p)$. The other vibrations in the considered wavenumber range correspond to the mixed $\delta(\phi_I) + \delta(\phi_p)$ modes.

The ν_{14} mode that corresponds to the asymmetric $\nu_{as}(\Phi)$ vibration of the entire skeleton has a peculiar nature among the in-plane stretching modes of 1*H*-imidazo[4,5-*c*]pyridine (Figure 6). In this vibration both rings mutually “breathe”; that is, the enlargement of one ring is associated with simultaneous shrinking of the second ring. The wavenumbers of these modes have been calculated at 1252–1257 cm^{−1}. In the IR spectrum the $\nu_{as}(\Phi)$ mode is observed at about 1258 cm^{−1}.

The second characteristic in-plane bending vibration of the imidazopyridine skeleton is described by the mode calculated at about 786 cm^{−1}. It is a characteristic type of vibration in which both rings breathe simultaneously, and therefore it is denoted as the $\nu_s(\Phi)$ symmetric mode (Figure 6). The $\nu_s(\Phi)$ vibration is observed in the 798–808 cm^{−1} range. Its intensity in the Raman spectrum is significantly higher than its IR counterpart.

Out-of-Plane Modes of 1*H*-Imidazo[4,5-*c*]pyridine.

Eleven out-of-plane bending vibrations of IPc are observed in the 200–964 cm^{−1} range, corresponding to the following modes: $\gamma(\text{CH})_p$ at 963–964, 904–905, 818 cm^{−1}; $\gamma(\text{CH})_I$ at 840 cm^{−1}; $\gamma(\phi_p) + \gamma(\phi_I)$ at 776, 598–606 cm^{−1}; $\gamma(\phi_I)$ at 632–645 cm^{−1}; $\gamma(\phi_p)$ at 232–238 cm^{−1}; $\gamma(\text{NH})$ at 423–437 cm^{−1}.

Among the out-of-plane modes there is a characteristic vibration of the imidazopyridine skeleton. The ν_{36} mode calculated at about 220 cm^{−1} should be denoted as the $\tau(\Phi)$ -wagging motion of the entire skeleton. The ν_{34} ($\gamma(\Phi)$ -waving mode) calculated at about 410 cm^{−1} has been observed in the IR spectrum at 414 cm^{−1} and in the Raman spectrum at 416 cm^{−1} (Figure 6).

Vibrational Characteristics of the Hydrogen Bond in 1*H*-Imidazo[4,5-*c*]pyridine. N–H...N hydrogen bonds (HBs) play an important role in chemistry and biology. Benzoimidazoles are known to be strongly associated through intermolecular hydrogen bonding. Such interactions are expected for the IPc derivatives. The formation of the N₁–H...N_p HB is postulated by the XRD data. For the solid state in which such interactions appear, the N–H...N hydrogen bond is formed between the adjacent IPc units of the unit cell. A strong

Table 2. Experimental and Scaled Wavenumbers of the Vibrational Spectra for 1*H*-Imidazo[4,5-*c*]pyridine Monomer and Dimer^a

ν_n	experimental wavenumbers		calculated wavenumbers		PED contributions	
	IR	RS	monomer	dimer	monomer	dimer
ν_1	3408 wb		3517	3515	100 $\nu(\text{NH})_I$	100 $\nu(\text{NH})_I$
ν_2	3125 m		3106	3109, 3099	99 $\nu(\text{CH})_I$	99 $\nu(\text{CH})_I$
ν_3	3082 m	3075 s	3063	3071, 3061	99 $\nu(\text{CH})_P$	99 $\nu(\text{CH})_P$
ν_4	3043 m	3042 m	3037	3048, 3044	98 $\nu(\text{CH})_P$	98 $\nu(\text{CH})_P$
ν_5	3014 m	3015 m	3032	3029, 3023	100 $\nu(\text{CH})_P$	96 $\nu(\text{CH})_P$
	3000–1800	2931vw 2894 vw		3125		100 $\nu(\text{NH})_B$: stretching $\nu(\text{N-H}\cdots\text{N})$ HB vibration
ν_6	1620 m	1623 w	1603	1606, 1605	49 $\nu(\phi_P) + 21 \nu(\phi_I)$	46 $\nu(\phi_P) + 16 \nu(\phi_I)$
ν_7	1588 m	1588 m 1557 vw	1561	1568, 1562	45 $\nu(\phi_P) + 22 \nu(\phi_{P+I})$	50 $\nu(\phi_P) + 21 \nu(\phi_{P+I})$
	1493 m	1494 s		1486		32 $\nu(\text{C=N})_I + 17 \delta(\text{NH})_B + 13 \nu(\phi_P) + 11 \delta(\text{CH})_I$: in plane-bending $\delta(\text{N-H}\cdots\text{N})$ HB vibration
ν_8	1470 m	1471 m	1484	1484	54 $\nu(\text{C=N})_I + 17 \delta(\text{CH})_I$	53 $\nu(\text{C=N})_I + 16 \delta(\text{CH})_I + 14 \nu(\phi_P)$
ν_9	1460 shm		1445	1450, 1445	44 $\delta(\text{CH})_P + 22 \nu(\phi_P) + 16 \nu(\phi_{P+I})$	44 $\delta(\text{CH})_P + 16 \nu(\phi_{P+I}) + 17 \nu(\phi_P)$
ν_{10}	1430 s	1430 m	1428	1433, 1406	32 $\nu(\phi_P) + 24 \delta(\text{CH})_P$	32 $\nu(\phi_P) + 30 \delta(\text{CH})_P$
						40 $\delta(\text{CH})_P + 26 \nu(\phi_P) + 12 \delta(\text{NH})_B$: in plane-bending $\delta(\text{N-H}\cdots\text{N})$ HB vibration
ν_{11}	1351 vw	1353 vw	1374	1378	36 $\delta(\text{CH})_P + 30 \delta(\text{NH})_I + 19 \nu(\phi_I)$	32 $\delta(\text{NH})_I + 31 \delta(\text{CH})_P + 20 \nu(\phi_I)$
ν_{12}	1333 s	1332 s	1320	1324, 1323	26 $\delta(\text{CH})_I + 25 \nu(\phi_I) + 12 \nu(\text{C=N})_I + 11 \nu(\phi_P)$	19 $\delta(\text{CH})_I + 20 \nu(\phi_I) + 10 \nu(\text{C=N})_I + 10 \nu(\phi_P)$
ν_{13}	1305 w 1300 w 1293 s 1283 m	1305 vs 1295 s 1284 s	1277	1283, 1281	40 $\delta(\text{CH})_P + 39 \nu(\phi_P)$	46 $\delta(\text{CH})_P + 44 \nu(\phi_P)$
ν_{14}	1258 s	1259 m	1252	1257, 1254	38 $\nu(\phi_P) + 36 \nu(\phi_I) + 13 \delta(\text{CH})_P$: [$\nu_{as}(\Phi)$]	37 $\nu(\phi_I) + 29 \nu(\phi_P) + 16 \delta(\text{CH})_P$: [$\nu_{as}(\Phi)$]
ν_{15}	1242 m		1233	1244, 1238	23 $\nu(\phi_I) + 17 \delta(\text{CH})_I + 11 \nu(\text{C=N})_I + 11 \nu(\phi_P) + 11 \delta(\text{NH})_I$	21 $\nu(\phi_P) + 19 \delta(\text{CH})_I + 17 \nu(\text{C=N})_I + 15 \nu(\phi_I)$
ν_{16}	1188 m 1178 w 1170 w	1199 m 1178 m 1172 m	1173	1176, 1173	40 $\nu(\phi_P) + 39 \delta(\text{CH})_P + 10 \nu(\phi_I)$	34 $\delta(\text{CH})_P + 28 \nu(\phi_P) + 15 \nu(\phi_I)$
ν_{17}	1140 m	1149 m	1160	1163, 1161	38 $\delta(\phi_P) + 16 \delta(\text{CH})_I + 22 \nu(\phi_I)$	32 $\delta(\phi_P) + 15 \nu(\phi_I) + 10 \delta(\text{CH})_I + 13 \nu(\phi_P)$
		1141 shm				
ν_{18}		1047 shm	1051	1097, 1050	63 $\nu(\text{N-C})_I + 26 \delta(\text{NH})_I$	65 $\nu(\text{N-C})_I + 25 \delta(\text{NH})_I$
ν_{19}	1031 m	1033 s	1019	1025, 1018	63 $\nu(\phi_P) + 26 \delta(\text{CH})_P$	63 $\nu(\phi_P) + 28 \delta(\text{CH})_P$
ν_{20}	963 m	964 m	952	952, 948	95 $\gamma(\text{CH})_P$	95 $\gamma(\text{CH})_P$
ν_{21}	928 m	929 m	922	924	67 $\delta(\phi_I) + 21 \nu(\phi_{P+I})$	61 $\delta(\phi_I) + 19 \nu(\phi_{P+I})$
ν_{22}	904 w	905 w	919	922, 918	99 $\gamma(\text{CH})_P$	51 $\gamma(\text{CH})_P + 33 \delta(\phi_I)$
ν_{23}	891 w 860 w	888 w 856 vw	872	883, 873, 863	56 $\delta(\phi_P) + 23 \nu(\phi_I)$	49 $\delta(\phi_P) + 21 \nu(\phi_I)$
						100 $\gamma(\text{NH})_B$: out-of-plane $\gamma(\text{NH}\cdots\text{N})$ HB vibration
ν_{24}	840 m	840 w	846	855, 852	85 $\gamma(\text{CH})_I + 13 \gamma(\phi_I)$	84 $\gamma(\text{CH})_I + 15 \gamma(\phi_I)$
ν_{25}	818 m		794	801, 798	92 $\gamma(\text{CH})_P$	92 $\gamma(\text{CH})_P$
ν_{26}	808 m 797 m	798 vs	786	788, 787	24 $\delta(\phi_P) + 32 \nu(\phi_P) + 23 \nu(\phi_I)$: [$\nu_s(\Phi)$]	37 $\nu(\phi_P) + 22 \nu(\phi_I) + 21 \delta(\phi_P)$: [$\nu_s(\Phi)$]
ν_{27}	776 w		773	777, 775	58 $\gamma(\phi_P) + 38 \gamma(\phi_I)$	59 $\gamma(\phi_P) + 39 \gamma(\phi_I)$
ν_{28}	636 s	645 m 632 m	642	642, 635	64 $\gamma(\phi_I) + 15 \gamma(\phi_P)$	70 $\gamma(\phi_I) + 21 \gamma(\phi_P)$
ν_{29}			621	626, 621	42 $\delta(\phi_I) + 29 \delta(\phi_P) + 22 \nu(\phi_P)$	39 $\delta(\phi_I) + 24 \delta(\phi_P) + 19 \nu(\phi_P)$
ν_{30}	606 vw 603 vw 598 w	605 w 599 w	600	601, 591	57 $\gamma(\phi_P) + 41 \gamma(\phi_I)$	48 $\gamma(\phi_P) + 44 \gamma(\phi_I)$
ν_{31}	566 m	560 m	547	556, 548	60 $\delta(\phi_P) + 15 \nu(\phi_I) + 14 \nu(\phi_P)$	57 $\delta(\phi_P) + 12 \nu(\phi_P) + 14 \nu(\phi_I)$

Table 2. continued

ν_n	experimental wavenumbers		calculated wavenumbers		PED contributions	
	IR	RS	monomer	dimer	monomer	dimer
	559 w					
ν_{32}	436 m 423 m	437 vw 425 vw	421	440	71 $\gamma(\text{NH})_1$ + 21 $\gamma(\phi_p)$	92 $\gamma(\text{NH})_1$
ν_{33}	417 shm		406	412, 407	60 $\delta(\phi_p)$ + 12 $\nu(\phi_1)$	57 $\delta(\phi_p)$ + 12 $\nu(\phi_1)$
ν_{34}	414 m	416 vw	404	412, 410	70 $\gamma(\phi_p)$ + 13 $\gamma(\phi_p \setminus \phi_1)$: [$\gamma(\Phi)$ -wagging]	75 $\gamma(\phi_p)$ + 12 $\gamma(\phi_p \setminus \phi_1)$: [$\gamma(\Phi)$ -wagging]
ν_{35}			243	249, 248	66 $\gamma(\phi_p)$ + 30 $\gamma(\phi_1)$	65 $\gamma(\phi_p)$ + 30 $\gamma(\phi_1)$
ν_{36}	232 w	238 w	215	222, 221	66 $\gamma(\phi_p \setminus \phi_1)$ + 22 $\gamma(\phi_p)$: [$\tau(\Phi)$ -wagging of the whole molecule]	66 $\gamma(\phi_p \setminus \phi_1)$ + 19 $\gamma(\phi_p)$: [$\tau(\Phi)$ -wagging of the whole molecule]
	113 w	113 s		84		89 $\nu(\text{NH}_B) \cdots \text{N}$: stretching $\nu(\text{N}-\text{H} \cdots \text{N})$ HB vibration
	106 w			70		100 $\delta(\text{NH}_B\text{N})$
				55		100 $\gamma(\text{NH}_B\text{N})$
				37		100 $\delta(\text{NH}_B\text{N})$
				13, 12		100 $\gamma(\text{NH}_B\text{N})$

^aCalculated values were scaled using the factors 0.96 for ν_1 – ν_5 and 0.97 for ν_6 – ν_{36} . ϕ_p , pyridine ring; ϕ_1 , imidazole ring; Φ , pyridine and imidazole ring; ν , stretching; δ , in-plane bending vibrations; γ , τ , out-of plane bending; H_B , hydrogen atom engaged in the HB; H_I , hydrogen atom of the imidazole ring (free for the dimer).

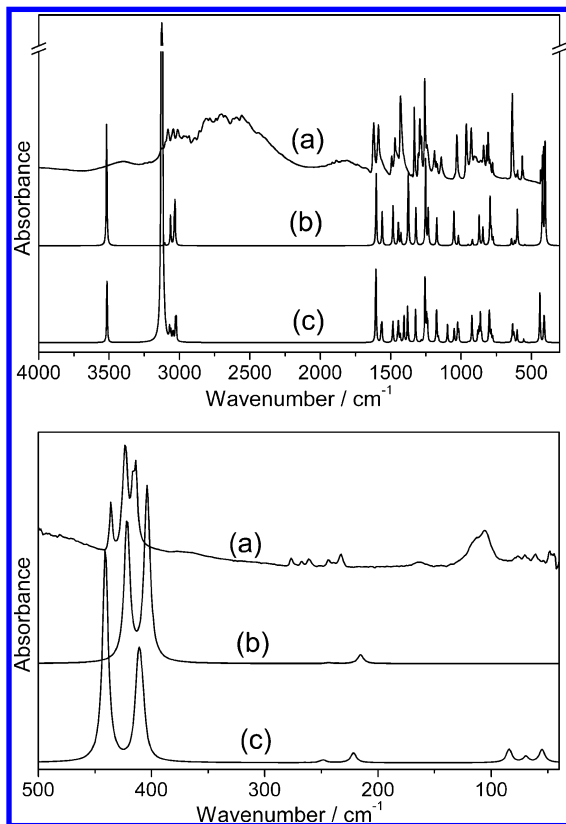


Figure 3. IR spectra of 1H-imidazo[4,5-c]pyridine: (a) experimental; (b) theoretical – calculated for the monomer; (c) theoretical – calculated for the dimer.

HB is formed between the N–H donor of the imidazole ring and nitrogen acceptor of the pyridine ring.

The theoretical calculations of IPC presented in this paper were performed for both the monomer and dimer. The characteristic vibrations of the HB for the dimer are predicted by the DFT calculations at the following wavenumbers: $\nu(\text{N}_1-\text{H} \cdots \text{N}_p)$ 3125 cm^{-1} ; $\delta(\text{N}_1-\text{H} \cdots \text{N}_p)$ at 1486 and 1406 cm^{-1} ; $\gamma(\text{N}_1-\text{H} \cdots \text{N}_p)$ at 863 cm^{-1} ; as well as $\nu(\text{N}_1-\text{H}) \cdots \text{N}_p$ at 84

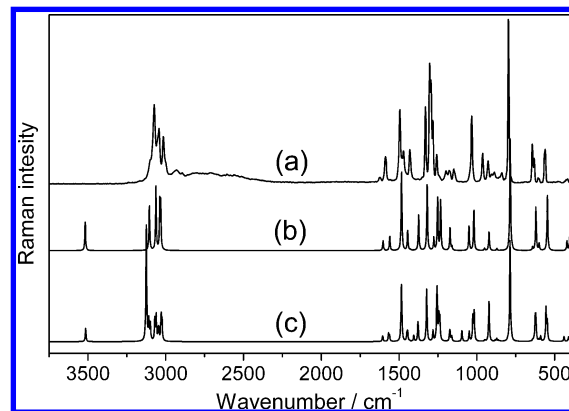


Figure 4. Raman spectra of 1H-imidazo[4,5-c]pyridine: (a) experimental; (b) theoretical – calculated for the monomer; (c) theoretical – calculated for the dimer.

cm^{-1} . These data agree well with the wavenumbers calculated for methyl derivatives of 1H-imidazo[4,5-c]pyridine.²⁵

The N–H stretch for the IPC derivatives is expected in the range characteristic for secondary amines, i.e., 3300–3500 cm^{-1} .^{25–27} The calculations show that the $\nu(\text{NH})$ stretching mode of such compounds should be observed at about 3515 cm^{-1} (Table 2). The NH group vibrations also contribute to several other modes. For instance, the ν_{11} , ν_{15} , and ν_{18} modes are mixed with the $\delta(\text{NH})$ vibration and the ν_{32} and ν_{34} modes with the $\gamma(\text{NH})$ vibration. These values were calculated using the noninteracting molecule approximation. However, such an assumption could not be used for these compounds in the solid state. The IR spectra of IPC show a broad and strong contour in the 1600–3500 cm^{-1} range (Figure 3). This contour contains a separate band at about 3410 cm^{-1} and a multiplet in the range 3200–1600 cm^{-1} . The latter contour can be deconvoluted into four Lorentzian components (see Figure 7). Three components of this multiplet form a typical ABC contour, in which the A-component appears at 2774 cm^{-1} , B at 2540 cm^{-1} , and C at 1812 cm^{-1} . Such system of bands is characteristic for the strong HB of the N–H \cdots O type formed between the imidazole N(3) nitrogen atom and oxygen atom of the H₂O molecule. The N(3) \cdots O_w distance derived from the XRD studies is 2.88 Å,

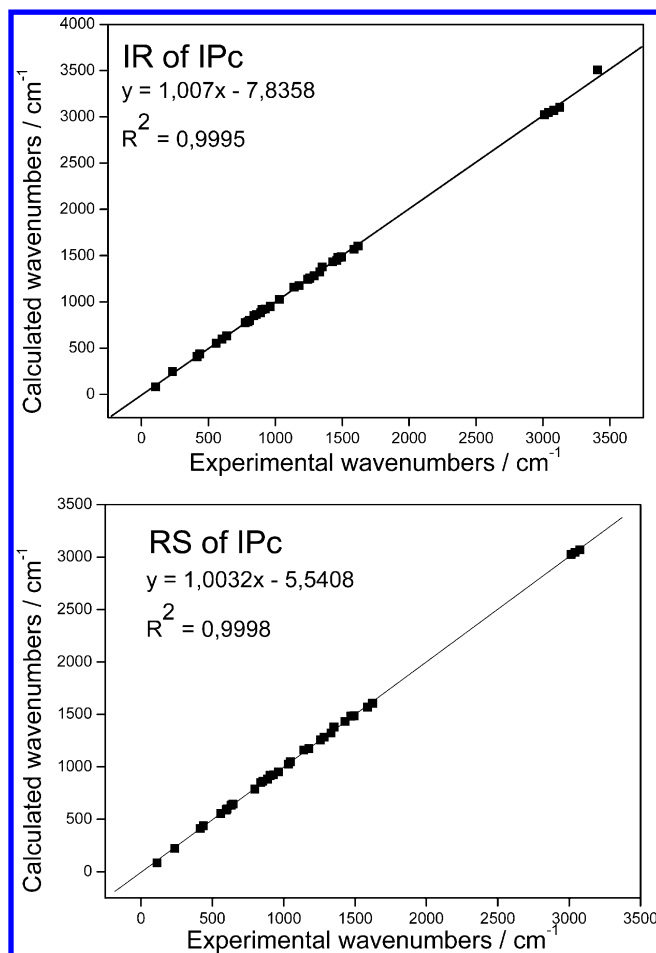


Figure 5. Comparison of the experimental and calculated FT-IR and FT-Raman spectra of 1H-imidazo[4,5-c]pyridine dimer.

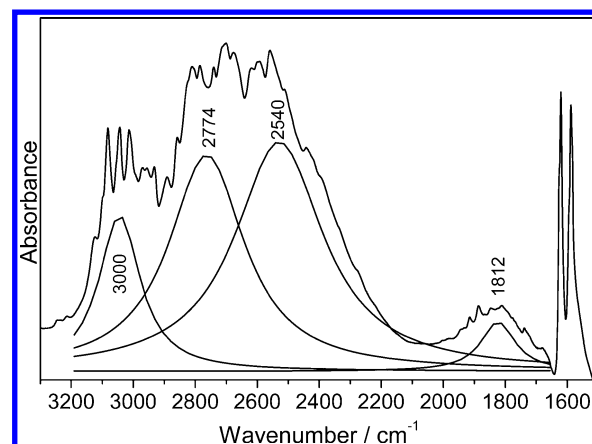


Figure 7. Lorentzian components of the 3200–1700 cm^{-1} band for 1H-imidazo[4,5-c]pyridine.

permitting classification of this HB as a moderately strong interaction. The fourth component, at about 3000 cm^{-1} , corresponds to the multiplet of the $\nu(\text{CH})$ vibrations overlapped with the N–H···N vibrations. These results confirm the data reported in our previous papers.^{25,27}

Vibrational Properties of Compounds Containing the Imidazopyridine Skeleton. Figure 8 shows the IR and Raman spectra of compounds containing the imidazopyridine unit: ABT-491 hydrochloride (ABT-491), 3-deazaadenosine (DZA), and 3-deazaneplanocin A hydrochloride (DZNep) (Figure 9). These compounds are widely used as pharmaceuticals. Two coupled rings form a system that has some characteristic vibrations: stretching $\nu_{\text{as}}(\Phi)$ and $\nu_{\text{s}}(\Phi)$ and wagging $\gamma(\Phi)$.

For compounds containing the imidazopyridine skeleton the $\nu_{\text{as}}(\Phi)$ vibration is observed at $1247\text{--}1260 \text{ cm}^{-1}$ and for IPc at

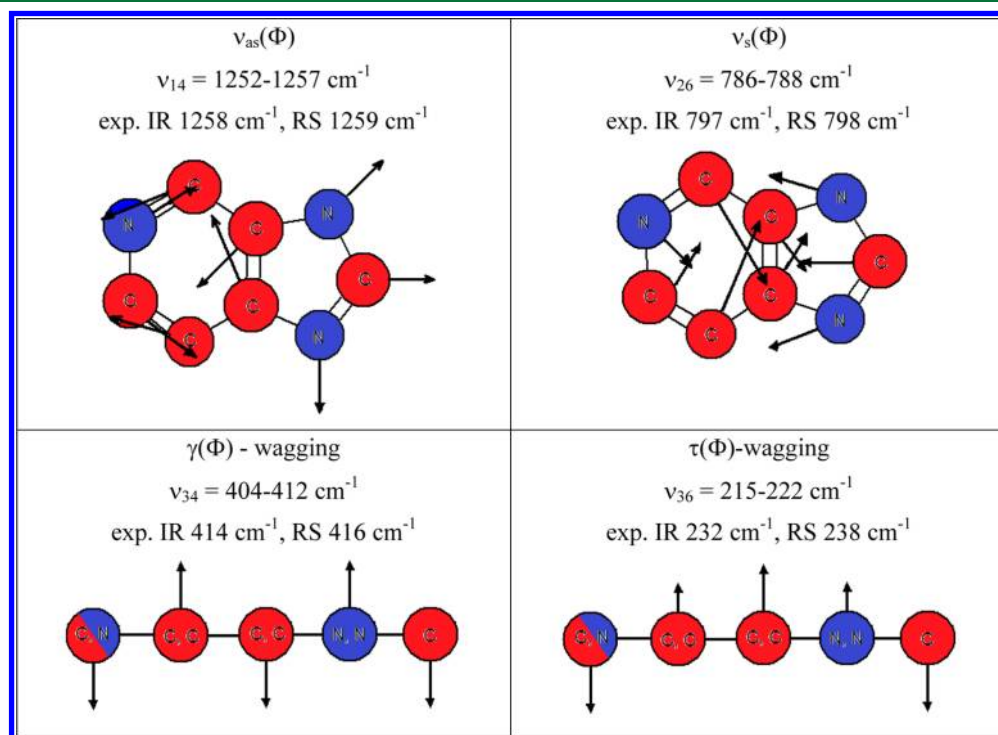


Figure 6. Chosen normal modes and the respective calculated and experimental wavenumbers of IPc rings.

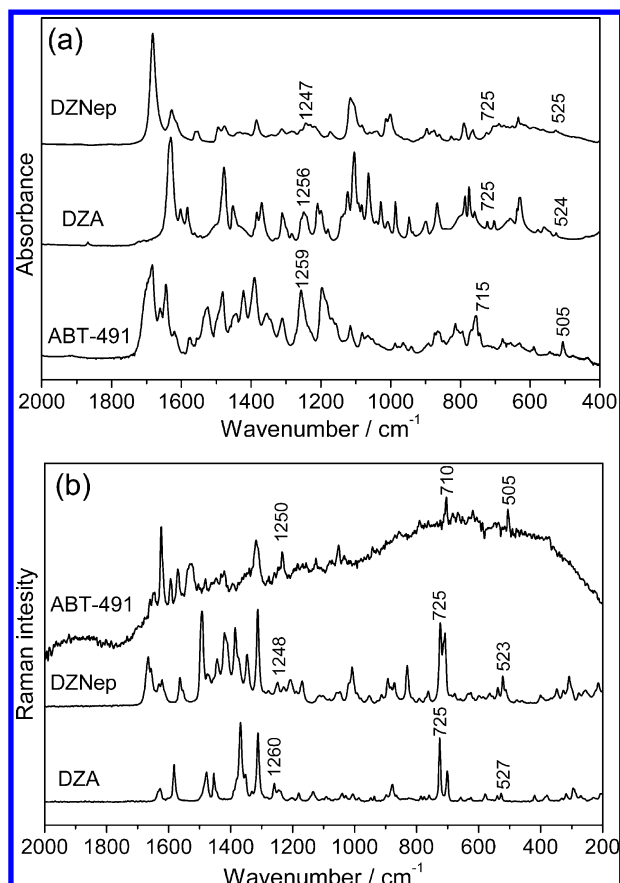


Figure 8. IR (a) and Raman (b) spectra of ABT-491 hydrochloride (ABT-491), 3-deazaadenosine (DZA), and 3-deazaneplanocin A (DZNep).

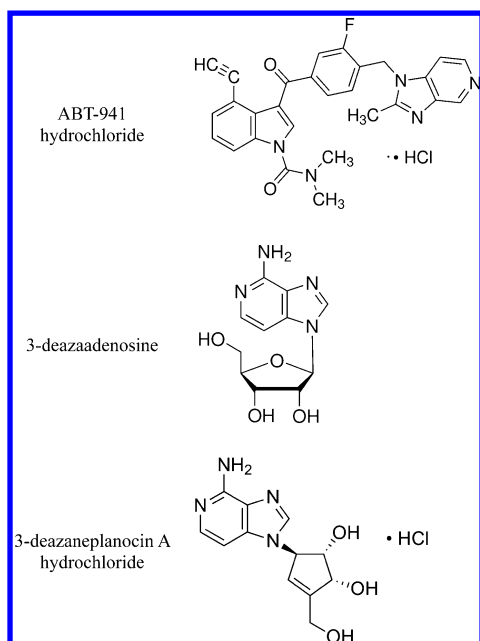


Figure 9. Structures of ABT-491, DZA, and DZNep.

1258–1259 cm^{-1} . The wavenumbers observed for the $\nu_s(\Phi)$ vibration shift toward lower wavenumbers (710–725 cm^{-1}) compared with the IPc vibration. The same trend appears for methyl derivatives of IPc discussed in our previous paper.²⁵ For the $\gamma(\Phi)$ -wagging vibration wavenumbers are higher for the

discussed compounds (505–525 cm^{-1}) than for IPc. For methyl derivatives of IPc this mode is observed in the same range, 502–526 cm^{-1} .²⁵ These vibrations could be used as a diagnostic tool for other systems containing the IPc unit.

Atomic Charges. The charge distribution of IPc allows comparison of the properties of the monomer and dimer. Pyridine and imidazole nitrogen and hydrogen atoms participate in the HB interactions between the IPc units of the dimer. Dimer formation implies changes in the charge distribution.

The calculated natural charges of the imidazole nitrogen (N-1), pyridine nitrogen (N-5), and hydrogen atoms are presented in Figure 10. Participation of N-1, N-5, and H atoms in an intramolecular charge transfer is revealed in the natural bond orbital (NBO) analysis. The formation of the dimer causes the charge increase of the hydrogen atom from 0.409e for the monomer to 0.444e for the dimer. The pyridine nitrogen atom is more negatively charged for the dimer (−0.529e) than for the monomer (−0.469e). This is the result of the charge transfer from hydrogen to the pyridine nitrogen atom in the dimer.

NBO Analysis. The NBO method is useful to characterize intra- and intermolecular bonding. The second-order Fock matrix was carried out to evaluate the donor–acceptor interactions in the NBO analysis.³⁰ The interaction causes the loss of occupancy from the localized NBO of the idealized Lewis structure into an empty non-Lewis orbital. For each donor (*i*) and acceptor (*j*), the stabilization energy $E^{(2)}$ associated with the delocalization $i \rightarrow j$ is estimated as

$$E^{(2)} = \Delta E_{ij} = q_i \frac{F(i, j)^2}{\epsilon_j - \epsilon_i}$$

where q_i is the donor orbital occupancy, ϵ_i and ϵ_j are diagonal elements (orbital energies), and $F(i, j)$ is the off-diagonal NBO Fock matrix element. Some electron donor orbital, acceptor orbital, and the interacting stabilization energy resulted from the second-order-microdisturbance theory.³⁰ The larger the $E^{(2)}$ value, the more intensive the interaction between electron donors and electron acceptors, i.e., the more donating tendency from electron donors to electron acceptors and the greater the extent of conjugation of the whole system.

A useful aspect of the NBO method is that it gives information about intra- and intermolecular bonding and interactions among bonds and also provides a convenient basis for investigating the interactions in both filled and virtual orbital spaces along with charge transfer and conjugative interactions in a molecular system.

The intermolecular N–H⋯N hydrogen bond as a strong interaction is exposed in the NBO analysis by the interaction between the N lone pair and N–H antibonding orbital ($N_p \rightarrow N_1-H$). This $E^{(2)} = 62.39 \text{ kJ/mol}^{-1}$ value is chemically significant and can be used as a measure of the intermolecular delocalization. However, the same effect obtained from the N lone pair of molecule II to the (C–C) antibonding orbital, N-5 \rightarrow C(6)–C(7) and N-5 \rightarrow C(9)–C(4), has the energetic contributions 37.58 and 37.12 kJ/mol, respectively.

Methyl derivatives of IPc were studied in our previous paper. A strong hydrogen bond was evident between the adjacent IPc molecules. The N–H donor of the imidazole ring and pyridine nitrogen acceptor were engaged in this bonding. The formation of a $N_1-H \cdots N_p$ HB was postulated by XRD data. Comparison of the data obtained in the NBO analysis for IPc derivatives with those obtained for free IPc shows similarity in $E^{(2)}$

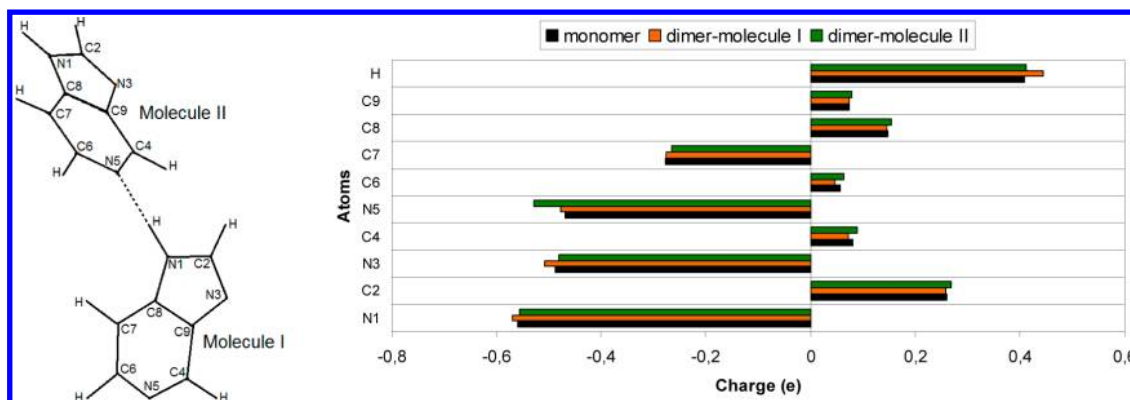


Figure 10. Molecular model used in the DFT calculations (A). Atomic charge distribution of monomer and dimer 1*H*-imidazo[4,5-*c*]pyridine: molecule I and molecule II (B).

energies, 62.76 kJ/mol⁻¹ for 4MIPc and 62.14 kJ/mol⁻¹ for 7MIPc.

The IPc dimer exhibits strong intramolecular hyperconjugative interactions of π -electrons with the greater energy contributions for molecule I from C(4)–N(5) \rightarrow C(8)–C(9) (50.55 kJ/mol), C(7)–C(6) (104.08 kJ/mol); C(8)–C(9) \rightarrow C(7)–C(6) (68.72 kJ/mol), C(2)–N(3) (60.72 kJ/mol); C(7)–C(6) \rightarrow C(4)–N(5) (61.65 kJ/mol), C(8)–C(9) (88.72 kJ/mol); C(2)–N(3) \rightarrow C(9)–C(8) (73.86 kJ/mol); and for molecule II: C(6)–C(7) \rightarrow N(5)–C(4) (60.14 kJ/mol), C(8)–C(9) (91.94 kJ/mol); C(8)–C(9) \rightarrow N(5)–C(4) (121.66 kJ/mol), C(6)–C(7) (67.17 kJ/mol).

Conclusions. The 1*H*-imidazo[4,5-*c*]pyridine skeleton is an important component of several natural and pharmaceutical products. FT-IR and FT-Raman spectroscopy techniques offer a fast diagnostic tool for detection of IPc. In the present paper the results of the spectroscopic and structural studies of IPc have been reported for the first time. Obtaining single crystals suitable for XRD diffraction by the method proposed in this paper enabled these studies. The comparative IR and Raman studies analyzed with the use of quantum chemical calculations allowed derivation of several characteristic vibrations from middle infrared (MIR) and “fingerprint” ranges that can be used for detection of the IPc skeleton in a new natural or synthetic product. Vibrational characteristics of the imidazopyridine double system exhibit several characteristic modes that remain nearly unchanged for the compounds containing this skeleton. These vibrations may be used as a diagnostic tool for other systems containing the imidazo[4,5-*c*]pyridine unit. The vibrational characteristics of this system contain the normal modes presented in Figure 6.

It should be noted that the N–H \cdots N hydrogen bond is formed in the systems containing IPc molecules, and their structures are stabilized by HBs between the proton of the imidazole ring (NH bond) and pyridine nitrogen of the adjacent molecule. The strength of such intermolecular interactions has been confirmed and estimated in the NBO calculations.

An interesting feature of the studied compound is the appearance in its 3-D framework of small channels that can be occupied by molecules of solvent or other small units. Therefore, the doping of such materials by foreign ions and molecules is possible.

EXPERIMENTAL SECTION

Synthesis. 1*H*-Imidazo[4,5-*c*]pyridine was obtained from 3,4-diaminopyridine. 3,4-Diaminopyridine (2.5 g) was dissolved in 10 mL of 100% formic acid, and the reaction mixture was boiled under reflux for 6 h. When formic acid was evaporated under reduced pressure, the next portion of 10 mL of formic acid was added, the reaction mixture was boiled under reflux for 6 h, and the formic acid was again evaporated under reduced pressure. Solid KHCO₃ (5 g) was added to the mixture, which was dried at 130 °C for 5 h. Water (20 mL) was added, the obtained solution was evaporated to dryness under reduced pressure, and the residue was dried at 110 °C for 4 h. The solid product was extracted with absolute EtOH, boiled with active carbon, and evaporated to dryness. EtOAc (50 mL) and a few milliliters of acetonitrile were added to the residue and boiled, and another portion of active carbon was added. The solution was filtered off and left for 72 h in a refrigerator. The product was recrystallized from EtOAc and dried at 110 °C. The melting point of the 1*H*-imidazo[4,5-*c*]pyridine was 169.5 °C, and the yield was 1.3 g, i.e., 48%. The product is well soluble in H₂O and EtOH. The molecular weight is 119.06 g. The results of its chemical analysis for the C₆H₅N₃ composition are C 60.04, H 4.41, N 35.10 wt %, and they are in good agreement with the expected composition (C 60.47, H 4.23, N 35.3 wt %).

IR and Raman Measurements. IR spectra in the 4000–30 cm⁻¹ range were recorded at room temperature using Nujol and Fluorolube suspensions and KBr pellet techniques with an FTIR BIORAD 575 spectrophotometer. The resolution was 2 cm⁻¹. Because all obtained spectra showed identical band contours, the spectra in a KBr disc have been presented in this paper as representative.

Raman spectra (RS) in the 4000–80 cm⁻¹ range were measured in back-scattering geometry with an FT Bruker 110/S spectrometer. The 1064 nm line of a Nd:YAG laser was used as excitation source. The resolution was 2 cm⁻¹. The Raman spectra were acquired using a typical container for the powdered samples.

Quantum Chemical Calculations. The molecular structures of the studied compound were optimized at the DFT level using the B3LYP^{31–33} and 6-311G(2d,2p) basis sets.^{34–40} Raman and IR wavenumbers as well as band intensities were calculated at the same DFT level using the GAUSSIAN 03W program.⁴¹ The calculated and experimental values were compared using scaling factors to correct the evaluated wavenumbers for vibrational anharmonicity and deficiencies inherent to the used computational level. A linear correlation was used for scaling the theoretical wavenumbers to compare them with the experimental values.^{42,43}

The intensities of the Raman lines in the theoretical spectra were corrected using the RAIN computer program⁴⁴ based on ref 45.

The AniMol program⁴⁶ was used for visualization of the vibrational normal modes and BALGA program⁴⁷ for estimation of the PED contributions of the internal coordinates to the normal modes.

The natural bond orbitals calculations were performed using the NBO program as implemented in the Gaussian 03W package at the

B3LYP/6-311G(2p,2d) level of theory in order to show a detailed description of the electronic structure of the IPC monomer and dimer.

X-ray Diffraction. Single-crystal X-ray diffraction was performed on a KM4-CCD diffractometer operating in κ geometry. Graphite-monochromated Mo $K\alpha$ radiation was used. The data were collected at 110 K in ω -scan mode with $\Delta\omega = 1.0^\circ$ using the CrysAlis CCD program.⁴⁸ RED software version 1.170.32 (Oxford Diffraction)⁴⁹ was used for data processing. An empirical absorption correction was applied using spherical harmonics implemented in the SCALE3 ABSPACK scaling algorithm. The structure was solved by direct methods and refined by the full-matrix least-squares method by means of the SHELX-97 program package.⁵⁰ All non-hydrogen atoms were refined anisotropically. The hydrogen atoms from C–H groups in IPC were generated geometrically (C–H 0.93 Å) and treated as riding atoms. The $U_{\text{iso}}(\text{H})$ values were constrained to be $1.2U_{\text{eq}}$ (carrier atom). The hydrogen atoms bonded to the N atom were localized at difference Fourier maps and refined with $U_{\text{iso}}(\text{H}) = 1.2U_{\text{eq}}$ of the corresponding parent atom. Due to the pronounced disorder of solvent molecules (H_2O and EtOH), the hydrogen atoms from these moieties were not introduced to the structure refinement. A possible arrangement of solvent molecules in the channels is presented in Figure S1 in the Supporting Information. Due to the fact that scattering factors of oxygen and carbon are similar and the degree of the disorder is high, the proposed model is only one of a many possible configurations. It minimizes well the electron density on difference Fourier maps, $\rho_{\text{max}} = 0.322$, $\rho_{\text{min}} = -0.232 \text{ e}/\text{\AA}^3$, and is the simplest one, with only one symmetrically independent position of ethanol in the unit cell. Different settings of molecules, however, as well as different EtOH to H_2O ratios cannot be excluded. CCDC 882076 contains the supplementary crystallographic data for this paper. The data can be obtained free of charge via www.ccdc.ac.uk.

■ ASSOCIATED CONTENT

● Supporting Information

A possible arrangement of solvent molecules in the channels. This material is available free of charge via the Internet at <http://pubs.acs.org>.

■ AUTHOR INFORMATION

Corresponding Author

*Tel: +48 71 3680299. Fax: +48 71 3680292. E-mail: lucyna.dyminska@ue.wroc.pl.

Notes

The authors declare no competing financial interest.

■ REFERENCES

- (1) Hishikawa, Y. *Asian Med. J.* **1991**, *34*, 578–585.
- (2) Leonard, B. E. In *Drug Treatment of Insomnia*; Leonard, B. E., Ed.; Fundamentals of Psychopharmacology; John Wiley: Chichester, 1992; pp 113–122.
- (3) Vaalamo, M.; Kariniemi, A. L.; Shapiro, S. D.; Saarialho-Kere, U. *J. Invest. Dermatol.* **1999**, *112*, 499–505.
- (4) Saarialho-Kere, U.; Kerkela, E.; Jeskanen, L.; Hasan, T.; Pierce, R.; Starcher, B. *J. Invest. Dermatol.* **1999**, *113*, 664–672.
- (5) Suomela, S.; Kariniemi, A. L.; Snellman, E.; Saarialho-Kere, U. *Exp. Dermatol.* **2001**, *10*, 175–183.
- (6) Matsumoto, S.; Kobayashi, T.; Katoh, M.; Saito, S.; Ikeda, Y.; Kobori, M. *Am. J. Pathol.* **1998**, *153*, 109–119.
- (7) Curci, J. A.; Liao, S.; Huffman, M. D.; Shapiro, S. D.; Thompson, R. W. *J. Clin. Invest.* **1998**, *102*, 1900–1910.
- (8) Corneliussen, L. A.; Nehring, L. C.; Harding, E.; Bolanowski, M.; Welgus, H. G.; Kobayashi, D. *J. Immunol.* **1998**, *161*, 6845–6852.
- (9) Kerkela, E.; Bohling, T.; Herva, R.; Uria, J. A.; Saarialho-Kere, U. *Bone* **2001**, *29*, 487–493.
- (10) Kerkela, E.; Ala-Aho, R.; Jeskanen, L.; Recharadt, O.; Grenman, R.; Shapiro, S. D. *J. Invest. Dermatol.* **2000**, *114*, 1113–1119.
- (11) Gordon, R. K.; Ginalski, K.; Rudnicki, W. R.; Rychlewski, L.; Pankaskie, M. C.; Bujnicki, J. M.; Chiang, P. K. *Eur. J. Biochem.* **2003**, *270*, 3507–3517.
- (12) Maki, A. S.; Kim, T. W.; Kool, E. T. *Biochemistry* **2004**, *43*, 1102–1110.
- (13) Cristalli, G.; Volpini, R. *Curr. Top. Med. Chem.* **2003**, *3*, 387–401.
- (14) Salvatori, D.; Volpini, R.; Vincenzetti, S.; Vita, A.; Costanzi, S.; Lambertucci, C.; Cristalli, G.; Vittori, S. *Bioorg. Med. Chem.* **2002**, *10*, 2973–2980.
- (15) Cristalli, G.; Costanzi, S.; Lambertucci, C.; Lupidi, G.; Vittori, S.; Volpini, R.; Camaioni, E. *Med. Res. Rev.* **2001**, *21*, 105–128.
- (16) Montgomery, J. A.; Clayton, S. J.; Thomas, H. J.; Shannon, W. M.; Arnett, G.; Bodner, A. J.; King, I.; Cantoni, G. L.; Chiang, P. K. *J. Med. Chem.* **1982**, *25*, 626–629.
- (17) Tseng, C. K. H.; Marquez, V. E.; Fuller, R. W.; Goldstein, B. M.; Haines, D. R.; McPherson, H.; Parsons, J. L.; Shannon, W. M.; Arnett, G.; Hollingshead, M.; Driscoll, J. S. *J. Med. Chem.* **1989**, *32*, 1442–1446.
- (18) Glazer, R. I.; Hartman, K. D.; Knode, M. C.; Richard, M. M.; Chiang, P. K.; Tseng, C. K. H.; Marquez, V. E. *Biochem. Biophys. Res. Commun.* **1986**, *135*, 688–694.
- (19) Arvanitis, A. G.; Rescinito, J. T.; Arnold, C. R.; Wilde, R. G.; Fitzgerald, L. W.; Zaczek, R.; Hartig, P. R.; Grossman, S.; Arneric, S. P.; Gilligan, P. J.; Olson, R. E.; Robertson, D. W. *Bioorg. Med. Chem. Lett.* **2003**, *13*, 129–131.
- (20) Heinrichs, S. C. *Curr. Opin. Drug Discovery Dev.* **1999**, *2*, 491–496.
- (21) Gilligan, P. J.; Robertson, D. W.; Zaczek, R. *J. Med. Chem.* **2000**, *43*, 1641–1660.
- (22) Gilligan, P. J.; Hartig, P. R.; Robertson, D. W.; Zaczek, R. In *Annual Report on Medicinal Chemistry*; Bristol, J. A., Ed.; Academic: San Diego, 1997; pp 41–50.
- (23) Flexner, C. W.; Hildreth, J. E.; Kuncl, R. W.; Drachman, D. B. *Lancet* **1992**, *339*, 438–443.
- (24) Albert, D. H.; Malo, P. E.; Tapang, P.; Shaughnessy, T. K.; Morgan, D. W.; Wegner, C. D.; Curtin, M. L.; Sheppard, G. S.; Xu, L.; Davidsen, S. K.; Summers, J. B.; Carter, G. W. *J. Pharmacol. Exp. Ther.* **1998**, *284*, 83–88.
- (25) Dymińska, L.; Gaęor, A.; Talik, Z.; Lorenc, J.; Hanuza, J. *Vib. Spectrosc.* **2011**, *57*, 229–241.
- (26) Dymińska, L.; Gaęor, A.; Mączka, M.; Węgliński, Z.; Hanuza, J. *J. Raman Spectrosc.* **2010**, *41*, 1021–1029.
- (27) Lorenc, J.; Dymińska, L.; Talik, Z.; Hanuza, J.; Mączka, M.; Wśkowska, A.; Macalik, L. *J. Raman Spectrosc.* **2008**, *39*, 1–15.
- (28) CCDC 882076 contains the supplementary crystallographic data for this paper. The data can be obtained free of charge via www.ccdc.ac.uk.
- (29) Singh, P.; May, J.; Townsend, L. B.; Hodgson, J. *J. Am. Chem. Soc.* **1976**, *98*, 825–830.
- (30) Weinhold, F.; Landis, C. R. *Valency and Bonding a Natural Bond Orbital Donor-Acceptor Perspective*; Cambridge University Press, 2005.
- (31) Lee, C.; Yang, W.; Parr, R. G. *Phys. Rev. B* **1988**, *41*, 785–789.
- (32) Becke, D. *J. Chem. Phys.* **1993**, *98*, 5648–5652.
- (33) Parr, R. G.; Yang, W. *Density-Functional Theory of Atoms and Molecules*; Oxford University Press: New York, 1989.
- (34) Ditchfield, R.; Hehre, W. J.; Pople, J. A. *J. Chem. Phys.* **1971**, *54*, 720–723.
- (35) Hehre, W. J.; Ditchfield, R.; Pople, J. A. *J. Chem. Phys.* **1972**, *56*, 2257–2261.
- (36) Hariharan, P. C.; Pople, J. A. *Theor. Chim. Acta* **1973**, *28*, 213–222.
- (37) Hariharan, P. C.; Pople, J. A. *Mol. Phys.* **1974**, *27*, 209–214.
- (38) Gordon, M. S. *Chem. Phys. Lett.* **1980**, *76*, 163–168.
- (39) Binning, R. C., Jr.; Curtis, L. A. *J. Comput. Chem.* **1990**, *11*, 1206–1216.
- (40) Frish, M. J.; Pople, J. A.; Binkley, J. S. *J. Chem. Phys.* **1984**, *80*, 3265–3269.

- (41) Frisch, M. J.; Trucks, G. W.; Schlegel, H. B.; Scuseria, G. E.; Robb, M. A.; Cheeseman, J. R.; Zakrzewski, V. G.; Montgomery, J. A., Jr.; Stratmann, R. E.; Burant, J. C.; Dapprich, S.; Millam, J. M.; Daniels, A. D.; Kudin, K. N.; Strain, M. C.; Farkas, O.; Tomasi, J.; Barone, V.; Cossi, M.; Cammi, R.; Mennucci, B.; Pomelli, C.; Adamo, C.; Clifford, S.; Ochterski, J.; Petersson, G. A.; Ayala, P. Y.; Cui, Q.; Morokuma, K.; Malick, D. K.; Rabuck, A. D.; Raghavachari, K.; Foresman, J. B.; Cioslowski, J.; Ortiz, J. V.; Baboul, A. G.; Stefanov, B. B.; Liu, G.; Liashenko, A.; Piskorz, P.; Komaromi, I.; Gomperts, R.; Martin, R. L.; Fox, D. J.; Keith, T.; Al-Laham, M. A.; Peng, C. Y.; Nanayakkara, A.; Challacombe, M.; Gill, P. M. W.; Johnson, B.; Chen, W.; Wong, M. W.; Andres, J. L.; Gonzalez, C.; Head-Gordon, M.; Replogle, E. S.; Pople, J. A. *GAUSSIAN 03*, Rev A. 1; Gaussian, Inc.: Pittsburgh, PA, 2003.
- (42) Scott, A. P.; Radom, L. *J. Phys. Chem.* **1996**, *100*, 16502–16513.
- (43) Palafox, M. A.; Rostogi, V. K. *Spectrochim. Acta, Part A* **2002**, *58*, 411–440.
- (44) Michalska, D. *RAINT (Raman Intensities), A Computer Program for Calculation of Raman Intensities from the Gaussian Outputs*; Wrocław University of Technology: Wrocław, 2002.
- (45) Michalska, D.; Wysokiński, R. *Chem. Phys. Lett.* **2005**, *403*, 211 and references therein.
- (46) Szcześniak, M. M.; Maślanka, B. *AniMol Computer Program: Infrared and Raman Spectroscopy Teaching and Research Tool*, Version 3.21; 1995–1997.
- (47) Rostkowska, H.; Łapiński, L.; Nowak, M. J. *Vib. Spectrosc.* **2009**, *49*, 43 (Nowak, M.; Łapiński, L. BALGA computer program for PED calculations).
- (48) Oxford Diffraction. *CrysAlis CCD*, Data Collection Software; Oxford Diffraction Ltd.: Wrocław, Poland, 2005.
- (49) Oxford Diffraction. *CrysAlis RED*, Data Reduction Program, Issue 171.32; Oxford Diffraction Ltd.: Wrocław, Poland, 2008.
- (50) Sheldrick, G. M. *Acta Crystallogr. A* **2008**, *64*, 112–122.